Cukurova University
Journal of
Natural & Applied Sciences

Original Paper

Investigation of Fatigue Behavior for Construction Vehicle Shafts

Furkan Çetin[1], Tolga Palanduz[1], Tuğrul Soyusinmez[1], Oğuzcan Güzelipek[1], Anıl Kaplan[1]

[1]Totomak Makine ve Yedek Parça San.Tic. A.Ş, İzmir/Turkey

ORCID IDs of the authors: F.Ç. 0000-0002-4805-4636; T.P. 0000-0001-7617-5825; T.S. 0000-0001-8333-1961; O.G. 0000-0001-5318-9204; A.K. 0000-0003-1143-8510.

Cite this article as: Çetin, F., Palanduz, T., Soyusinmez, T., Güzelipek, O., Kaplan, A. (2022). Investigation of Fatigue Behavior for Construction Vehicle Shafts, Cukurova University Journal of Natural & Applied Sciences 1(4): 1-12

Abstract

Induction surface hardened low alloyed medium carbon steels are frequently utilized in essential automotive and machine applications that demand high fatigue resistance. The right combination of hardening depth and the magnitude and distribution of residual compressive stresses in the surface layer determines the fatigue behavior of induction-hardened components to a large extent.

Axles are connected within vehicles to provide two vital functions: Carry torque from the engine to the wheels via a planetary gear arrangement, Keep the wheels in relative alignment with each other and the vehicle's body. The circular motion of the drive wheels is maintained in most noncommercial vehicles by axle shafts, which are an essential component of the rear axle. Two axle shafts, which are used as powertrain elements in construction vehicles hardened with induction heat treatment with SAE 4140 material standard, were broken during operation. In this study, 2 failed axle shafts and 2 non-failed axle shafts were compared in order to determine the reason for the breakage. The parts were cut from 3 different regions and the images of the pieces were taken with a CARL ZEIZZ NEOPHOT 32, NIKON SMZ 1500 light microscope. The microstructure and hardened case depths of the parts were checked. In microstructure images, it was seen that the structure was not completely homogeneous, However, it was understood that this was not the cause of the failure. And also, It was determined that the grain size of G1 and G2 shafts was rougher than T1 and T2. T shafts have been observed to have a low hardened case depth in the spline area. In the conical end area of the shafts, the prior austenite grain was found to be considerably coarser because the edge above the groove was overheated. Under the grove the inappropriate wave with decreasing oase-hardened depth have observed. It was determined that the reasons for the failure of the parts were low hardened depth. The effective case depths of the failed T-parts were found to be 6 mm, and the non-failed G-parts were greater than 8 mm. As a result of the studies, it was determined that the reason for the breakage of the parts was low hardened case depth caused by heat treatment

Keywords: Fatigue behavior, heat treatment, construction vehicle shaft, case hardening depth.

1. Introduction

A rotating shaft known as an axle is typically used to connect wheels and differentials in order to convey driving force and wheel movement. These shafts experience bending and torsional loads over the course of millions of cycles due to cyclic loading [1]. These axle shafts might fail from fatigue. Crack initiation, crack propagation, and fracture are the three stages of fatigue failure. About 90% of all service failures are caused by fatigue [2].

Where there is a concentration of stress, such as steps in diameter, grooves, keyways, threads, notches, press-fit components, and so on, fatigue failure begins. Metallurgical stress may form as a result of corrosion, inclusions, quench cracking, second-phasee particles, etc. [3].

Address for Correspondence:
Furkan Çetin, e-mail: fcetin@totomak.com.tr

Received: Dec 7, 2022
Accepted: Dec 14, 2022

Any component failure in a vehicle is usually a negative situation since it results in lost lives and financial damages. An automobile's axle shaft is a crucial part that transmits power to the wheels. A significant loss during transportation might result from the rear axle shaft failing or breaking. The fracture of the rear axle shaft was mostly caused by a poor keyway, spline, or other metallurgical design [4-11].

Induction surface hardened low alloyed medium carbon steels are frequently utilized for high fatigue-resistance crucial automotive and machine applications such propulsion shafts, crankshafts, and steering knuckles. The right balance of hardening depth, residual compressive stress magnitude, and distribution in the surface layer determines how induction-hardened objects will wear out [12-13].

The metalworking sector is currently expanding globally. Metal part fabrication or assembly procedures make up its main manufacturing processes. Electrical machinery (motors, generators, and transformers), other machinery (engines, turbines, pumps, mining and metalworking equipment), transportation equipment (automobiles, aircraft, railroad equipment, ships and boats), and other fabricated metal products are just a few of the many products that this industry produces. Each of these components has specific details that are utilized in situations like dynamic loads. Because there are ever more different components that operate under the impact of dynamic loads, it is important to adequately check their quality during both the production and operating processes. The unique construction of heavily loaded components provides the capacity to sustain loads without damage. Such components feature a moderate core material and a toughened surface layer. The case hardening depth is a component's quality criterion [14].

The case hardening depth that may be reached by utilizing induction hardening and appropriately choosing medium carbon low alloy steels can be significantly more than that of carburizing. Consequently, there is a large increase in torsion strength [15]. However, a deep case depth leads to a significant quench-ing deformation, which compromises dimensional accuracy. Applying the induction hardening method requires a precise balance between the case hardening depth, torsion strength, and quenching deformation. Many major businesses have started working on the induction hardening of cylindrical drive gear shafts recently [16].

2. Material and Method

Induction surface hardened low alloyed medium carbon steels are frequently utilized in essential automotive and machine applications that demand high fatigue resistance. The right combination of hardening depth and the magnitude and distribution of residual compressive stresses in the surface layer determines the fatigue behavior of induction-hardened components to a large extent.

Axles are connected within vehicles to provide two vital functions:

- Carry torque from the engine to the wheels via a planetary gear arrangement,
- Keep the wheels in relative alignment with each other and the vehicle's body. The circular motion of the drive wheels is maintained in most noncommercial vehicles by axle shafts, which are an essential component of the rear axle.

Two axle shafts, which are used as powertrain elements in construction machines hardened with induction heat treatment with SAE 4140H material stand-ard, were broken during operation. In this study, 2 failed axle shafts and 2 non-failed axle shafts were compared in order to determine the reason for the breakage.

Pieces were cut in regions A, B, C, and images were taken with a CARL ZEIZZ NEOPHOT 32, NIKON SMZ 1500 light microscope. The microstructure structure and hardened case depths of the parts were checked.

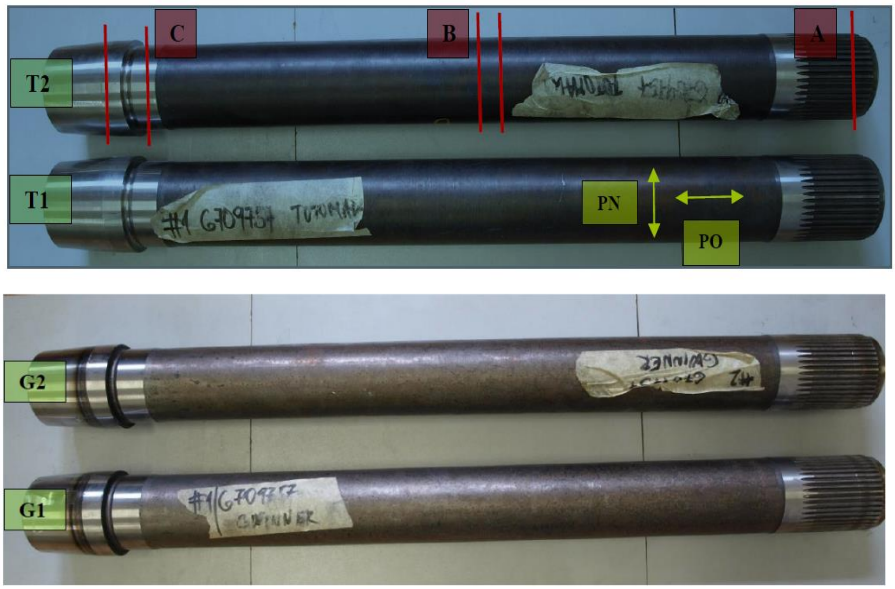

Figure 1. Parts for analysis with cutting positions, directions, and designation

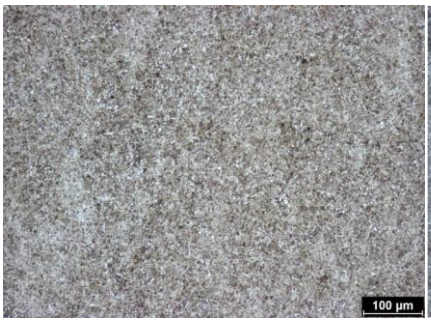

Figure 2.a A-PN – tooth, hardened layer

(martensite, retained austenite < 5 %)

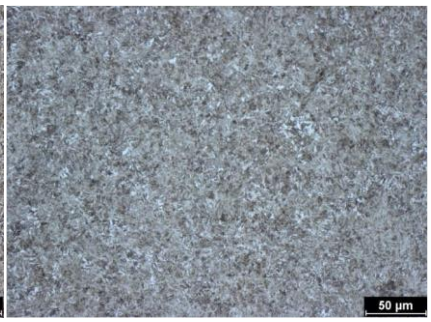

Figure 2.b A-PN – tooth, hardened layer (detail) G (Grain Size Number) = 7 (sample T1)

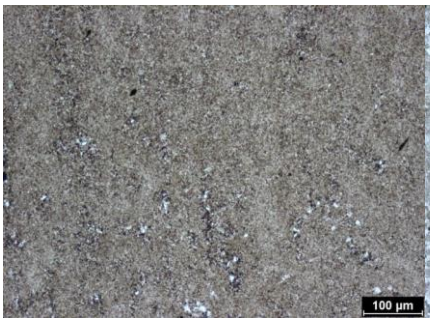

Figure 3. A-PN – transition zone
(mixture of martensite, pearlite and ferrite)

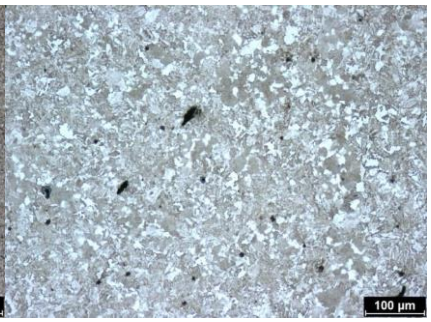

A-PN – unaffected core (sample T2)
G (Grain Size Number) = 5.5 (pearlite and ferrite, needle ferrite 50/35/15)

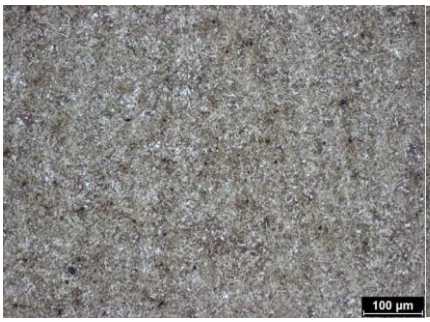

Figure 4.a
B-PN – hardened layer
(Martensite, retained austenite < 5 %)

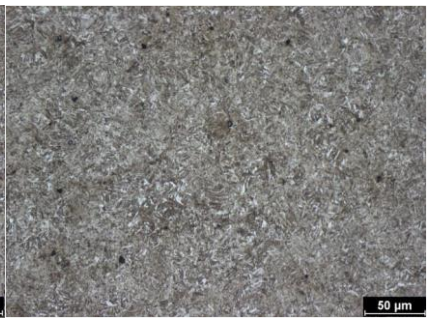

Figure 4.b
B-PN – hardened layer (detail)
G(Grain Size Number) = 7 (sample T1)

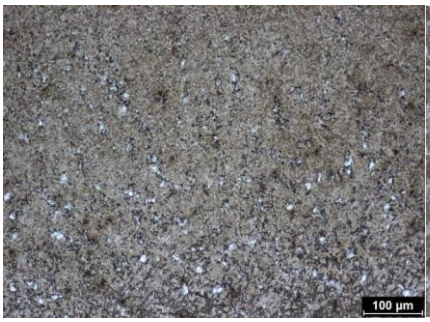

Figure 5.a
B-PN – transition zone
(Mixture of martensite, pearlite and ferrite)

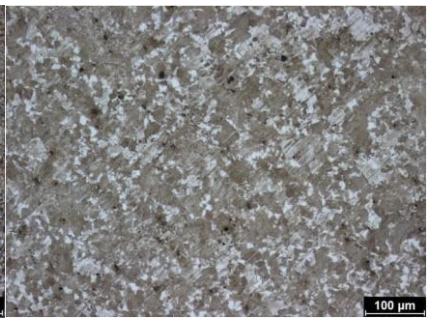

Figure 5.b
B-PN – unaffected core (sample T2)
G (Grain Size Number) = 5 (pearlite and ferrite, 50/50)

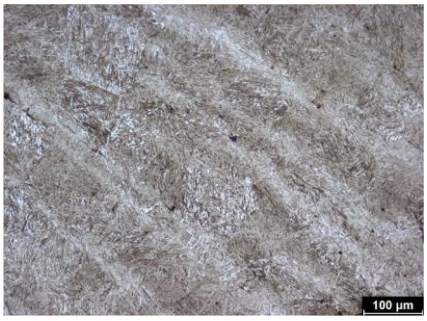

Figure 6.a
C-PO – hardened layer
G (Grain Size Number) = 3.5
(coarsed martensite, retained austenite)

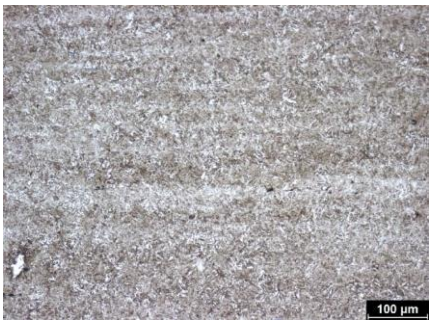

Figure 6.b
C-PO – hardened layer
G (Grain Size Number) = 7.5 (sample T1)
(fine martensite, retained austenite ~ 5 %)

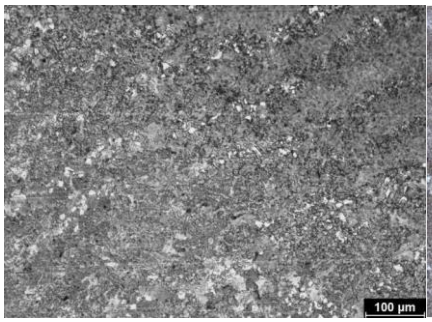

Figure 7.a
C-PO – transition zone
(mixture of martensite, pearlite and ferrite)

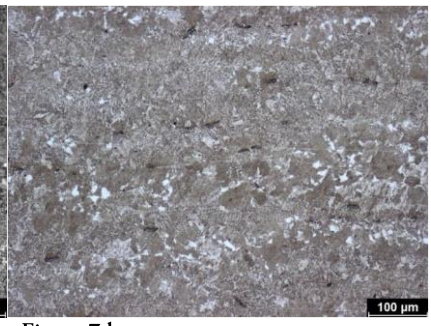

Figure 7.b
C-PO – unaffected core (sample T2)
G (Grain Size Number) = 5.5
(pearlite and ferrite, needle ferrite 50/10/40)

The data in the Tables 1-10 show how the particle size on the surface and core of the material is in the A, B and C sections of each sample. Particle size data on the surface and core of the material helps us see whether the microstructure is homogeneous. The values in Table 1-10 show the core grain size in A, B and C regions for each sample. The grain size values on the surface and core of the material were checked to see if the microstructure was homogeneous.

Table 1. Grain size number G of prior austenitic grain – sample T1

Sample	A PN	B PN	C PN
Quenched Surface	7	7	3.5-7.5
Core	5.5	5	5.5

Table 2. Grain size number G of prior austenitic grain – sample T2

Sample	A PN	B PN	C PN
Quenched Surface	7	7	3.5-7.5
Core	5.5	5.5	5.5

Table 3. Grain size number G of prior austenitic grain – sample G1

Sample	A PN	B PN	C PN
Quenched Surface	6.5	3.5	2.5-5
Core	6	4	3

Table 4. Grain size number G of prior austenitic grain – sample G2

Sample	A PN	B PN	C PN
Quenched Surface	5.5	6.5	3-5
Core	5	4	5

Table 5. Surface hardness measurement HRC T1 And T2

Measurement site	T1		T2	
	A	B	A	B
1	52	53,5	51	54
2	53	54	52	55
3	54	53,5	51	54
4	53	55	51	54
5	53	54	51	53,5
Average Value	53 ±0.5	54 ±0.5	51 ±0.5	54 ±0.5

Table 6. Surface hardness measurement HRC G1 and G2

Measurement site	G1		G2	
	A	B	A	B
1	56	52	55	51
2	55	52	56	52
3	56	51	56	52
4	55	51	55,5	50,5
5	55	51	55,5	51
Average Value	55.5 ±0.5	51.5 ±0.5	55.5 ±0.5	51 ±0.5

Table 7. Hardness measurement from the edge to core in HV1

Distance From Edge (mm)	T1		
	A PN	B PN	B PO
0,15	554	581	568
0,3	595	572	568
0,45	605	586	572
0,6	555	595	586
0,75	586	595	568
0,9	581	605	550
1,15	605	590	577
1,4	590	581	563
1,65	572	600	572
1,9	563	572	555
2,4	559	577	542
2,9	563	586	568
3,4	443	559	559
3,9	247	581	568

4,15	239	559	550
4,4	236	542	542
4,65	239	496	496
4,9	242	307	440
5,15	241	241	269
5,4	252	262	233
5,65	243	250	230

Table 8. Hardness measurement from the edge to core in HV1

Distance From Edge (mm)	T2		
	A PN	B PN	B PO
0,15	534	572	568
0,3	577	559	568
0,45	581	550	572
0,6	559	538	586
0,75	568	568	568
0,9	581	605	550
1,15	605	590	577
1,4	590	581	563
1,65	572	600	572
1,9	563	572	555
2,4	559	577	542
2,9	563	586	568
3,4	443	559	559
3,9	247	581	568
4,15	239	559	550
4,4	236	542	542
4,65	254	264	496
4,9	243	287	440
5,15	243	243	269
5,4	246	248	233
5,65	248	251	230

Table 9. Hardness measurement from the edge to core in HV1

Distance From Edge (mm)	G1		
	A PN	B PN	B PO
0,15	624	530	538
0,3	672	546	538
0,45	656	530	542

0,6	634	546	538
0,75	590	568	530
0,9	534	550	534
1,15	341	555	546
1,4	254	550	538
1,65	234	590	546
1,9	240	550	550
2,4	248	577	568
2,9	250	577	572
3,4	248	586	590
3,9	258	555	586
4,15	254	577	586
4,4	252	572	600
4,65	251	503	619
4,9	259	455	595
5,15	266	455	605
5,4	269	550	614
5,65	263	514	600
5,9	270	452	403
6,15		308	254
6,4		229	252
6,65		229	256
6,9		233	256
7,15		254	269
7,4		225	284
7,65		239	269
7,9		224	277

Table 10. Hardness measurement from the edge to core in HV1

Distance From Edge (mm)	G2		
	A PN	B PN	B PO
0,15	605	530	550
0,3	614	546	559
0,45	633	530	550
0,6	624	546	550
0,75	619	568	559
0,9	614	550	555
1,15	629	555	563

1,4	619	550	581
1,65	629	590	581
1,9	608	550	586
2,4	385	577	609
2,9	290	577	586
3,4	327	586	595
3,9	345	555	619
4,15	305	577	586
4,4	325	572	352
4,65	333	503	572
4,9	290	455	559
5,15	321	455	600
5,4	329	550	434
5,65	333	514	485
5,9	316	452	371
6,15		308	300
6,4		229	254
6,65		229	252
6,9		233	260
7,15		254	251
7,4		225	251
7,65		239	259
7,9		224	256

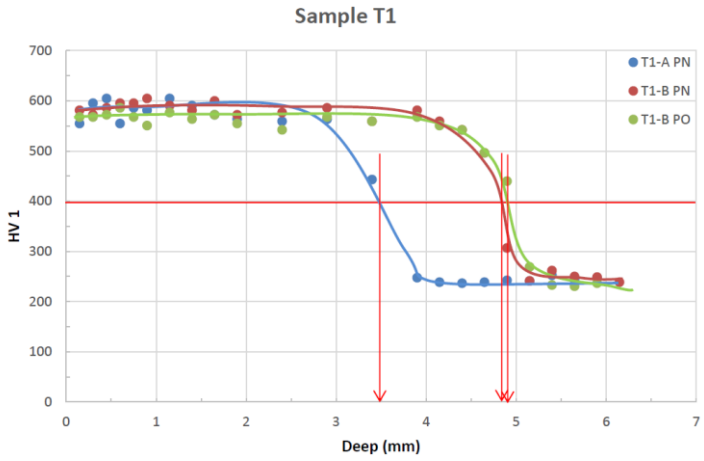

Figure 8. Hardness profile from surface to core and effective case depth of sample T1

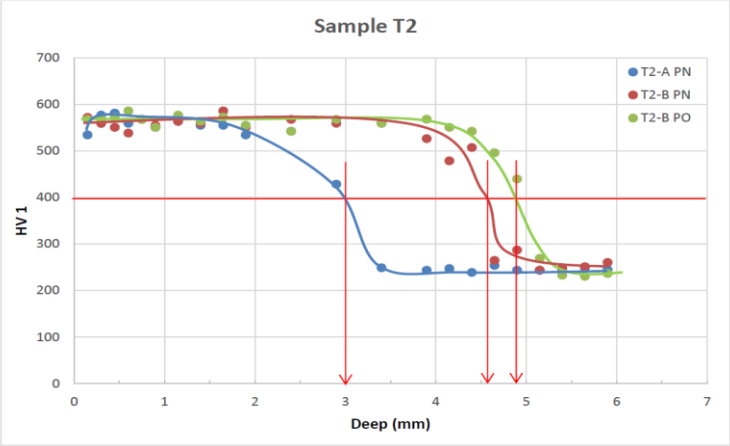

Figure 9. Hardness profile from surface to core and effective case depth of sample T2

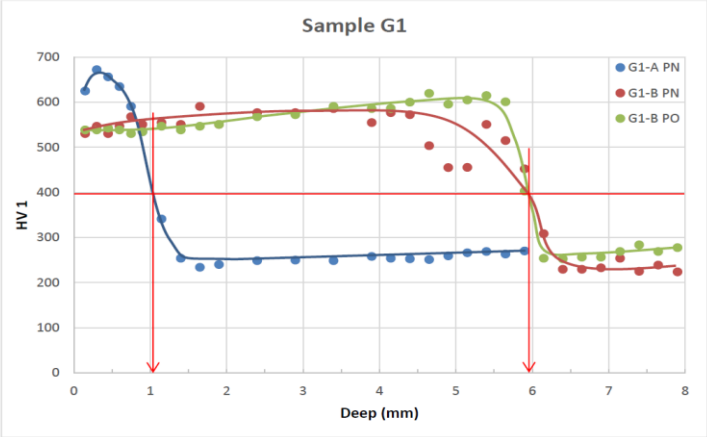

Figure 10. Hardness profile from surface to core and effective case depth of sample G1

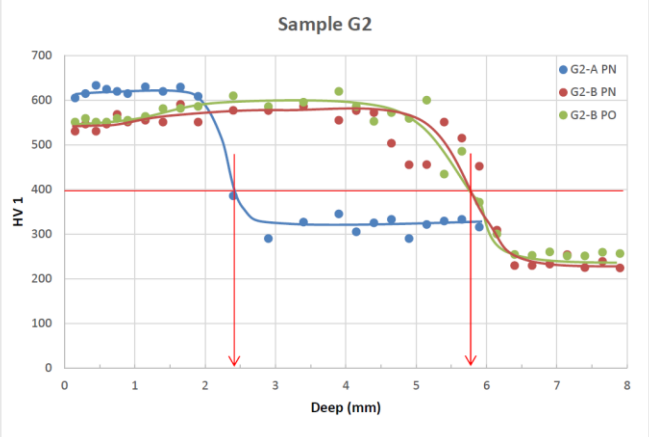

Figure 11. Hardness profile from surface to core and effective case depth of sample G2

Table 11. Effective Case Depth of the Samples

Sample	Total heat affected zone depth	Effective case depth calculated as 75% of heat-affected zone depth	Effective case depth hardness of 40 HRC (392 HV)
T1-A PN	3.67(Fig. 7)	2.75	3.5
T1-B PN	4.74(Fig. 7)	3.55	4.8
T1-B PO	4.93(Fig. 7)	3.7	4.9
T2-A PN	3.15(Fig. 8)	2.4	3
T2-B PN	4.83(Fig. 8)	3.6	4.6
T2-B PO	5.15(Fig. 8)	3.9	4.8
G1-A PN	1.2(Fig. 9)	0.9	1.05
G1-B PN	6.09 (Fig. 9)	4.6	5.9
G1-B PO	6.14 (Fig. 9)	4.6	5.9
G2-A PN	2.58 (Fig. 10)	1.9	2.4
G2-B PN	5.79 (Fig. 10)	4.3	5.75
G2-B PO	6.32 (Fig. 10)	4.75	5.75

Higher effective case depth may be acceptable. Significantly low effective case depth in A section of all shafts is influenced by inappropriate positioning of inductor in spline end of the shafts.

Table 12. Chemical composition of the samples

Element	SAE 4140H	T1	T2	G1	G2
Carbon	0,37-0,44	0,43	0,42	0,45	0,45
Manganese	0,65-1,10	0,86	0,85	0,88	0,86
Phosporus	0,035 max	0,014	0,013	0,012	0,01
Sulfur	0,040 max	0,021	0,022	0,012	0,009
Silicon	0,15-0,35	0,37	0,36	0,23	0,23
Chromium	0,75-1,20	1,11	1,10	1,01	1,00
Molybdenum	0,15-0,25	0,0223	0,22	0,21	0,21

Higher content of carbon, silicon and sulfur than required in the specification does not affect significantly the properties of used steel.

3. Results

In the tests carried out after the heat treatment of the shafts, it has been observed that T shafts do not provide the necessary qualifications to operate without breaking. It was determined that the micropurity and chemical compositions of the steel were suitable for all shafts. It was observed that the microstructures of the T shaft steels were not homogene-ous, and the grain size of the shafts is rough. Based on the tests carried out It was observed that, T shafts have low hardened case depth in area of spline (section A). In area of conical end of shafts (section C), the edge over the grove was overheated and prior austenite grain is significantly coarser than required. Under the grove the inappropriate wave with de-creasing of case-hardened depth is evident. Shafts have significant shift in start of induction hardening on the spline region (section A), due to, the effective case-hardened depth is insufficient and undesirable free ferrite occurring in microstructure. In area of the conical end of shafts (section C), the edge over the grove was overheated and prior austenite grain is significantly coarser than required.

References

[1] Chaudhary, S. K., Rajak, A. K., Ashish , K. (2021). Failure analysis of rear axle shaft of a heavy vehicle. Materials Today: Proceedings 38 : 2235-2240.

[2] Colangelo, V. J., & Heiser, F. (1974). Analysis of Metallurgical Failures.(Retroactive Coverage). John Wiley & Sons, Inc., 1974,, 361.

[3] Chaudhary, S. K., Rajak, A. K., & Ashish, K. (2021). Failure analysis of rear axle shaft of a heavy vehicle. Materials Today: Proceedings, 38, 2235-2240.

[4] Nanaware , G.K., Pable, M.J. (2003). Failures of rear axle shafts of 575 DI tractors. Eng. Fail. Anal. 10 (6) 719–724.

[5] Asi, O. (2006). Fatigue failure of a rear axle shaft of an automobile. Engineering failure analysis, 13(8), 1293-1302.

[6] Van Zyl, G., Al-Sahli, A. (2013). Failure analysis of conveyor pulley shaft. Case Stud. Eng. Fail. Anal. 1 (2) 144–155.

[7] Jinfeng, D., Liang, J., Zhang, L. (2016) . Research on the failure of the induced draft fan's shaft in a power boiler. Case Stud. Eng. Fail. Anal. 5 (6) 51–58.

[8] Xiaolei, X., Zhiwei,Y. (2009).Failure analysis of a locomotive turbocharger mainshaft. Volume 16, Issue 1, p 495-502.

[9] Lancha ,A.M., Serrano, M., Lapeña, J., Gómez-Briceño, D. (2001). Failure analysis of a river water circulating pump shaft from a NPP. Eng. Fail. Anal. 8 (3) 271–291.

[10] Momcˇilovic´, D. , Odanovic´, Z., Mitrovic´, R., Atanasovska, I.,Vuherer, T. (2012). Failure analysis of hydraulic turbine shaft. Eng. Fail. Anal. 20 54–66.

[11] Fuller, R.W., Ehrgott, J.Q., Heard, W.F., Robert, S.D., Stinson, R.D., Solanki, K., Hor-stemeyer ,M.F. (2008).Failure analysis of AISI 304 stainless steel shaft. Eng. Fail. Anal. 15 (7) 835–846.

[12] Xu, D.H. , Kuang, Z.B. (1996). A study on the distribution of residual stress due to surface induc-tion hardening. J Eng Mats Tech Ž. Trans ASME ; 118:571-575.

[13] Semiatin, S. L., & Stutz, D. E. (1986). Induction Heat Treatment of Steel, American Society for Metals, Metals Park, OH, Carnes Publication Services.

[14] Salchak, Y. A. Sednev D. A., Kroening, M. Ardashkin, I. B. (2015). Method of case hardening depth testing by using multi-functional ultrasonic testing instrument. IOP Conference Series: Materials Science and Engineering. Vol. 81. No. 1. IOP Publishing,

[15] Shen, Q., & Liang, W. (2008). Modern induction heat treatment technologies.

[16] Chen, B., Wang, D. P., Li, H. Y., Cui, K., & Jiang, B. (2017). Investigation on Induction Hardening Treatment of Cylindrical Drive Gear Shaft. In Society of Automotive Engineers (SAE)-China Congress (pp. 589-604). Springer, Singapore